

Structural evolution during the reduction of chemically derived graphene oxide

Akbar Bagri¹, Cecilia Mattevi^{2†}, Muge Acik³, Yves J. Chabal³, Manish Chhowalla^{2†} and Vivek B. Shenoy^{1*}

The excellent electrical, optical and mechanical properties of graphene have driven the search to find methods for its large-scale production, but established procedures (such as mechanical exfoliation or chemical vapour deposition) are not ideal for the manufacture of processable graphene sheets. An alternative method is the reduction of graphene oxide, a material that shares the same atomically thin structural framework as graphene, but bears oxygen-containing functional groups. Here we use molecular dynamics simulations to study the atomistic structure of progressively reduced graphene oxide. The chemical changes of oxygen-containing functional groups on the annealing of graphene oxide are elucidated and the simulations reveal the formation of highly stable carbonyl and ether groups that hinder its complete reduction to graphene. The calculations are supported by infrared and X-ray photoelectron spectroscopy measurements. Finally, more effective reduction treatments to improve the reduction of graphene oxide are proposed.

The chemical derivation of graphene oxide (GO) provides a high yield of covalently functionalized, atomically thin carbon sheets^{1,2}. GO recently emerged as a solution-processable material for large-area electronics because it can be deposited readily and uniformly on a variety of substrates^{3–5}. GO contains saturated sp^3 carbon atoms bound to oxygen, which makes it an insulator. Transition to a semiconductor through chemical or thermal removal of oxygen allows it to be reduced incrementally so that the electrical conductivity can be tuned over several orders of magnitude^{5–8}. However, reduced GO (rGO) still contains residual (~8 atomic per cent) oxygen that is sp^3 bonded to approximately 20% of the carbon atoms^{4,6}. The presence of these sp^3 sites disrupts the flow of charge carriers through sp^2 clusters so that transport in rGO occurs primarily by hopping rather than near ballistically, as in the case of mechanically exfoliated graphene^{9,10}. A clear trend between the optoelectronic properties (transparency, conductivity and mobility) is observed with increasing sp^2 fraction through removal of oxygen in GO. However, virtually all studies in the literature, which used a variety of reduction techniques^{4,6,11–13}, report the presence of residual oxygen in rGO. This represents a fundamental limitation that must be overcome if rGO is to achieve properties that resemble those of mechanically exfoliated graphene.

Crucially, our current knowledge of the bonding configuration or location of the residual oxygen is lacking. The necessary insight into why oxygen remains despite robust reduction treatments can be obtained if we identify the atomic positions and configurations of oxygen in rGO. Also lacking is information about the density and types of defects generated during oxygen evolution and the final hybridization states of C-C and C-O bonds and their spatial distribution.

We use molecular dynamics (MD) simulations to uncover the interplay between carbon and oxygen and the degree of defects and translational order of the residual atoms at different temperatures. This study at the atomistic level reveals that reduction by thermal treatment leads to the formation of carbonyl and ether groups. Calculations from first principles confirm that both

groups are stable thermodynamically and cannot be removed without destroying the parent graphene sheet. The MD simulations are supported by infrared absorption spectroscopy and X-ray photoelectron spectroscopy (XPS) taken during the thermal annealing.

Results and discussion

The oxygen functional groups on the graphene basal plane in GO consist of epoxy and hydroxyl molecules¹⁴, although evidence for the presence of ketones and phenols was also found², and edges can comprise carboxyls, anhydrides, lactones, phenols, lactols, pyrones and ketones^{15,16}. Although several models^{2,14,17–19} were proposed to describe GO, a coherent and detailed explanation of the structure needs to be elucidated. GO is not stoichiometric and is highly hygroscopic^{2,20}, and hence its composition can vary with the synthesis method^{2,21–24} and environment²⁰. Therefore, we performed MD simulations (see Methods) on GO sheets with variable oxygen contents of 16.6% (ref. 25), 20% (ref. 25), 25% (refs 20,26) and 33% (refs 21,22,26), values consistent with those reported in the literature. Also, we varied the ratio of hydroxyl to epoxy functional groups in the basal plane (1/1, 3/2 and 2/3). We took into account the experimental observation of Cai *et al.*²⁷, who found that a hydroxyl group bonded to a carbon atom was accompanied by an epoxy group bonded to a neighbouring carbon atom (see Supplementary Fig. S1). The annealing temperatures (1,000 K, 1,500 K, 1,600 K and 3,000 K) were selected to correlate with the XPS studies so that the simulated results could be compared with experimental data.

The initial configurations of GO sheets with oxygen atoms in hydroxyl and epoxy groups (in the ratio 3/2) considered in our simulations are shown in Supplementary Fig. S1. The structures of the sheets after annealing at 1,500 K are shown in Fig. 1a,b. It is clear that significant atomic rearrangement took place and that the GO sheets were substantially disordered after thermal annealing, with the highest initial oxygen-content structure being the most extreme case, as indicated in Fig. 1b. Specifically, carbonyls, linear carbon chains, ether rings (such as furans, pyrans and pyrones), 1,2-quinones, 1,4-quinones, five-member carbon rings, three-member

¹Division of Engineering, Brown University, Providence, Rhode Island 02912, USA, ²Rutgers University, Department of Materials Science and Engineering, Piscataway, New Jersey 08854 USA, ³Department of Materials Science and Engineering, University of Texas Dallas, Richardson, Texas 75080, USA;

[†]Present address: Department of Materials, Imperial College, London SW7 2AZ, UK. *e-mail: Vivek_Shenoy@brown.edu

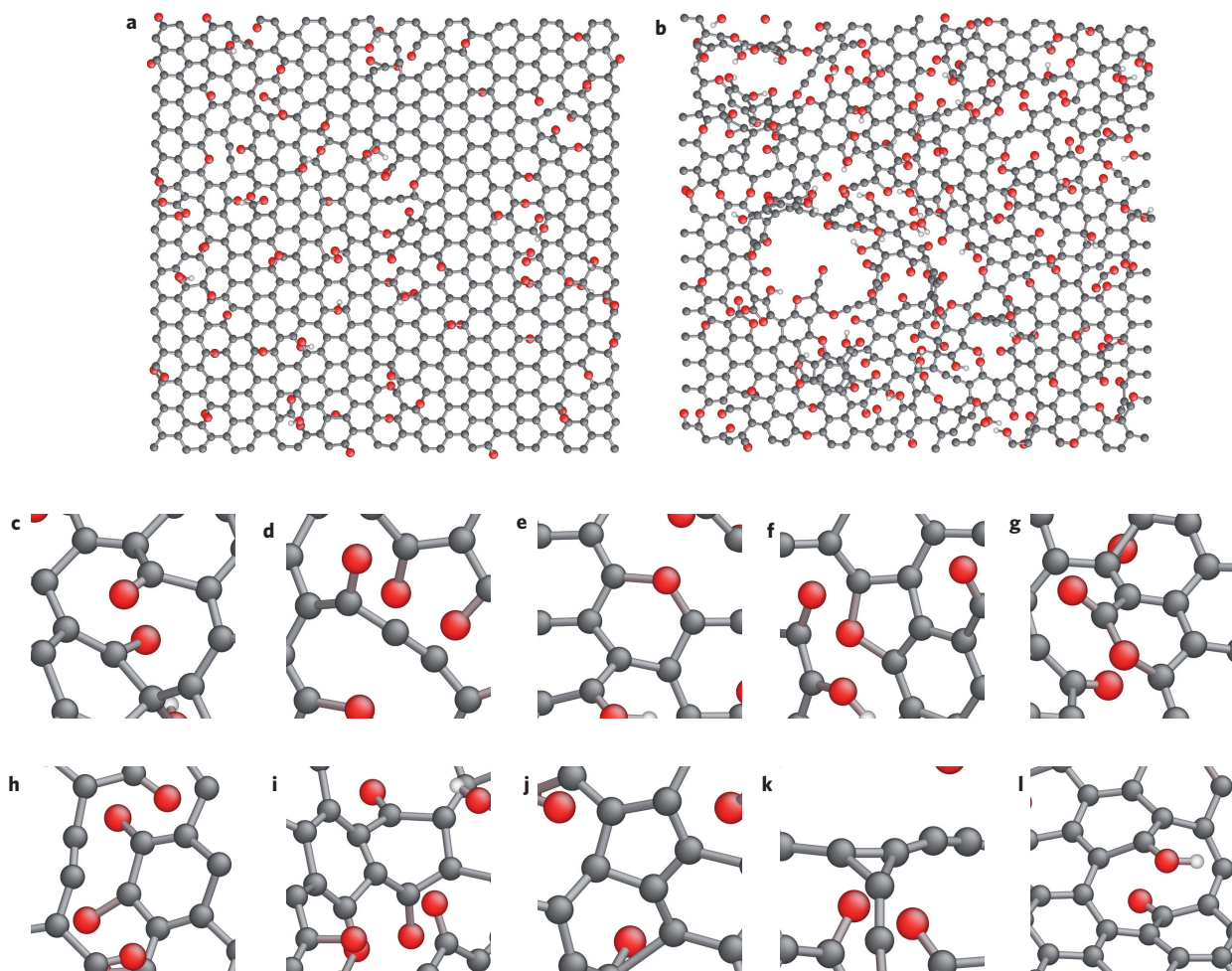


Figure 1 | Morphology of rGO and the structure of defects formed during thermal annealing. **a,b,** Morphology of rGO sheets with an initial oxygen concentration of 20% (**a**) and 33% (**b**) in the form of hydroxyl and epoxy groups in the ratio 3/2 after annealing at 1,500 K. The initial distribution of the functional groups in the two cases is shown in Supplementary Fig. S1b. **c–l,** Oxygen functional groups and carbon arrangements formed after annealing: a pair of carbonyls (**c**), carbon chain (**d**), pyran (**e**), furan (**f**), pyrone (**g**), 1,2-quinone (**h**), 1,4-quinone (**i**), five-member carbon ring (**j**), three-member carbon ring (**k**) and phenol (**l**). Carbon, oxygen and hydrogen atoms are grey, red and white, respectively.

carbon rings and phenols, along with increased sheet roughness, were evident (Fig. 1c–l and Supplementary Fig. S3).

Analysis of the MD simulations revealed that the hydroxyl functional groups required lower temperatures for desorption than the epoxy groups, as indicated by the release of H_2O below 1,000 K. Above this temperature, evolution of a small amount ($\sim 2\%$) of CO , CO_2 and O_2 was observed. O_2 evolution is attributed to desorption of some isolated epoxy groups and the release of CO_2 and CO was observed when hydroxyl and epoxy sites were in close proximity, a scenario readily observed at an oxygen concentration of 33%. The desorption of hydroxyls introduces minimal disorder within the honeycomb carbon lattice, as indicated by the lower concentration of vacancies and pentagonal rings at these sites. The desorption of epoxy groups in close proximity to other saturated sp^3 carbon bonds led to the creation of vacancies within the basal plane as a result of the evolution of CO_2 and CO molecules above 1,500 K.

The oxygen that remained in the rGO was dependent on the initial oxygen concentration, the hydroxyl/epoxy ratio and the annealing temperature, as indicated in Table 1. The efficiency of reduction was larger for lower initial oxygen concentrations (16.6% (not shown) and 20%) and the highest hydroxyl/epoxy ratio (3/2). This can be explained by the lower energy required to remove hydroxyls relative to that for epoxy groups and also because isolated epoxy groups are very stable. The concentrations

of functional groups that remained in the annealed GO versus the initial oxygen content are summarized in Fig. 2. The relative concentrations of the hydroxyl, carbonyl and ether groups increased with initial oxygen content at the expense of epoxy groups. Some residual hydroxyls were present as phenol groups (Fig. 1l), in agreement with experiments²⁸. However, at low initial oxygen concentrations (20%), isolated epoxy groups remained even after annealing up to 1,000 K.

Table 1 | Reduction efficiency of thermal annealing.

Initial O (%)	Final O (%)	
	1,000 K	1,500 K
20% (2:3)	18.7 (11.8)	15.4 (10.1)
20% (3:2)	16.3 (8.9)	13.6 (7.2)
25% (2:3)	23.1 (16.2)	20.5 (16.0)
25% (3:2)	20.7 (13.3)	17.3 (12.0)
33% (2:3)	29.7 (26.5)	28.9 (25.3)
33% (3:2)	29.7 (23.9)	24.9 (21.6)

Simulation results of oxygen concentration after heating GO with different initial oxygen concentrations. The percentage of oxygen atoms that remain after heating (1,000 K and 1,500 K) are given and the values in brackets correspond to the percentage of residual oxygen left behind after further annealing of rGO in a hydrogen atmosphere at the thermal reduction temperatures (1,000 K and 1,500 K). The ratios of hydroxyls/epoxy groups are given in parentheses for each initial oxygen concentration.

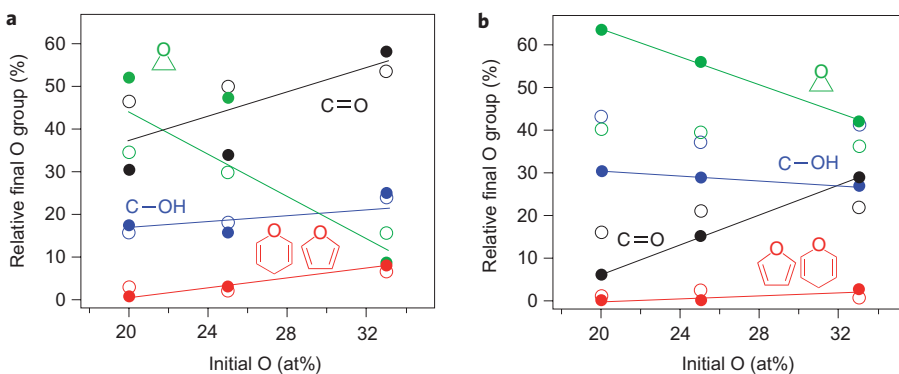


Figure 2 | Concentration of different functional groups in rGO. **a,b,** Concentrations of oxygen functional groups that remained in rGO after heating to 1,500 K (**a**) and 1,000 K (**b**) versus initial oxygen concentration. The functional groups are carbonyls (black), hydroxyls (blue), epoxy groups (green) and furan and pyran (red). Filled circles indicate an initial hydroxyl/epoxy ratio of 2/3, whereas the open circles refer to an initial ratio of 3/2. The lines are guides for the eye. at% = atomic per cent.

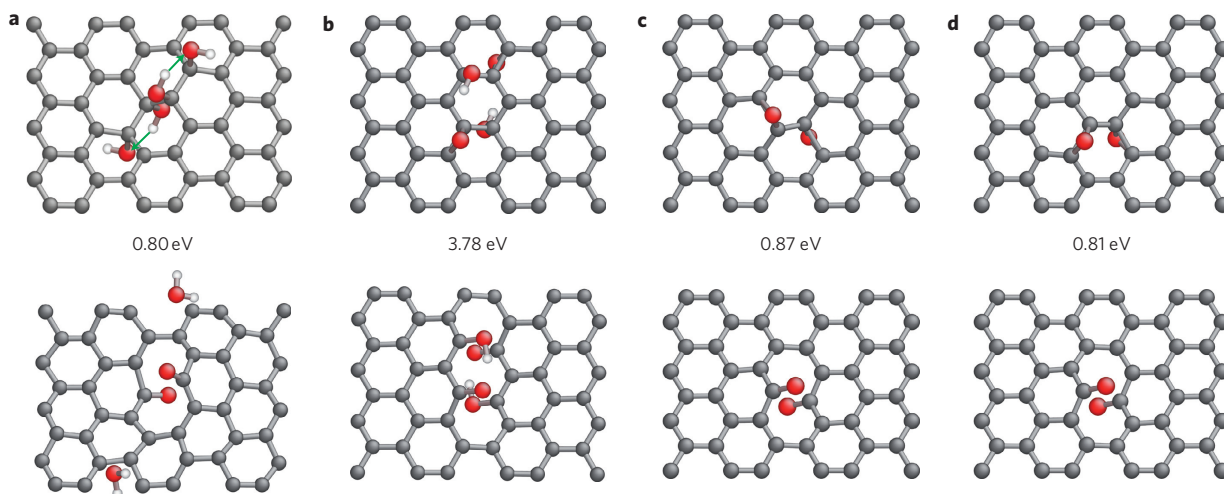


Figure 3 | Formation energies and structures of defects in rGO. **a-d,** Initial configuration of hydroxyl and epoxy groups (top) leads to the formation of carbonyl and phenol groups (bottom). **(a)** The transfer of hydrogen between neighbouring hydroxyl groups (indicated by green arrows) leads to the formation of a carbonyl pair. **b-d,** The strain created by epoxy groups leads to the creation of carbonyl and phenol groups that relax the strain in the vicinity of the neighbouring carbon atoms. The energy differences ($E_i - E_f$ (eV)) between the initial configurations (top) and the final configurations (bottom) are given, in each case obtained using DFT calculations (see Methods). The formation of these holes is energetically favourable in all cases. Carbon, oxygen and hydrogen atoms are shown as grey, red and white, respectively. The energy barriers and activated states for the transformation of a pair of epoxy groups to a pair of carbonyls and for the formation of a phenol–carbonyl pair from a hydroxyl and an epoxy are given in Supplementary Fig. S6.

The stability of isolated epoxy groups at this temperature is shown by the remarkably high percentage of residual epoxy (up to 63.5% are epoxy groups with only 7% carbonyls and 0% ethers), as illustrated in Fig. 2b.

Close examination of the residual oxygen revealed that the formation mechanisms of groups such as carbonyls (Fig. 1c) and ether rings (Fig. 1e,f) had different origins. Overall, carbonyls were created by rearrangement of epoxy groups and hydroxyls closely surrounded by saturated carbons (sp^3), but the formation of substitutional oxygen (C–O–C ether rings) was favoured at high temperatures. This is supported by the data plotted in Fig. 2b. Considering the concentration of each functional group after annealing at 1,000 K (Fig. 2b), the carbonyls concentration progressively increased (from 7–15% up to 20–28%), whereas epoxy concentration decreased (from 40–60% down to 37–42%). The effect was most prominent for GO with a hydroxyl/epoxy ratio of 2/3 (green filled circles in Fig. 2b). Although the increase in the initial oxygen concentration at 1,000 K led to an increase in carbonyl concentration, this was much more pronounced at higher temperatures (from 1,500–1,600 K up to 3,000 K), and reached a saturation value of 50%. The formation of

carbonyls can be linked to the interplay between hydroxyl and epoxy groups or to two epoxy groups bonded with two neighbouring carbon atoms and facing the opposite side of the sheet. The initial configurations of the oxygen groups that led to the formation of carbonyl- and hydroxyl-decorated, hole-like configurations are shown in Fig. 3. The generation of carbonyls in such configurations is favoured thermodynamically, as shown by the reduction in the total energy (indicated by the energy values given for each transition, see Methods) of the system on formation of these functional groups (Fig. 3). The relative stability of holes decorated by carbonyl pairs can be explained by the strain in the basal plane induced by different functional groups. The attachment of epoxy groups on graphene leads to a non-planar ‘frustrated’ sp^3 -bonding configuration for carbon atoms connected to oxygen, which in turn creates significant strain in neighbouring C–C bonds, which may affect their infrared activity (infrared absorption by the C–C stretch modes at $\sim 1,550\text{ cm}^{-1}$). However, in the case of a hole with a carbonyl pair, the bonding configuration remains close to planar sp^2 hybridization because of the formation of C=O bonds, which leads to little strain in the basal plane. A hole with a carbonyl pair is therefore a relatively

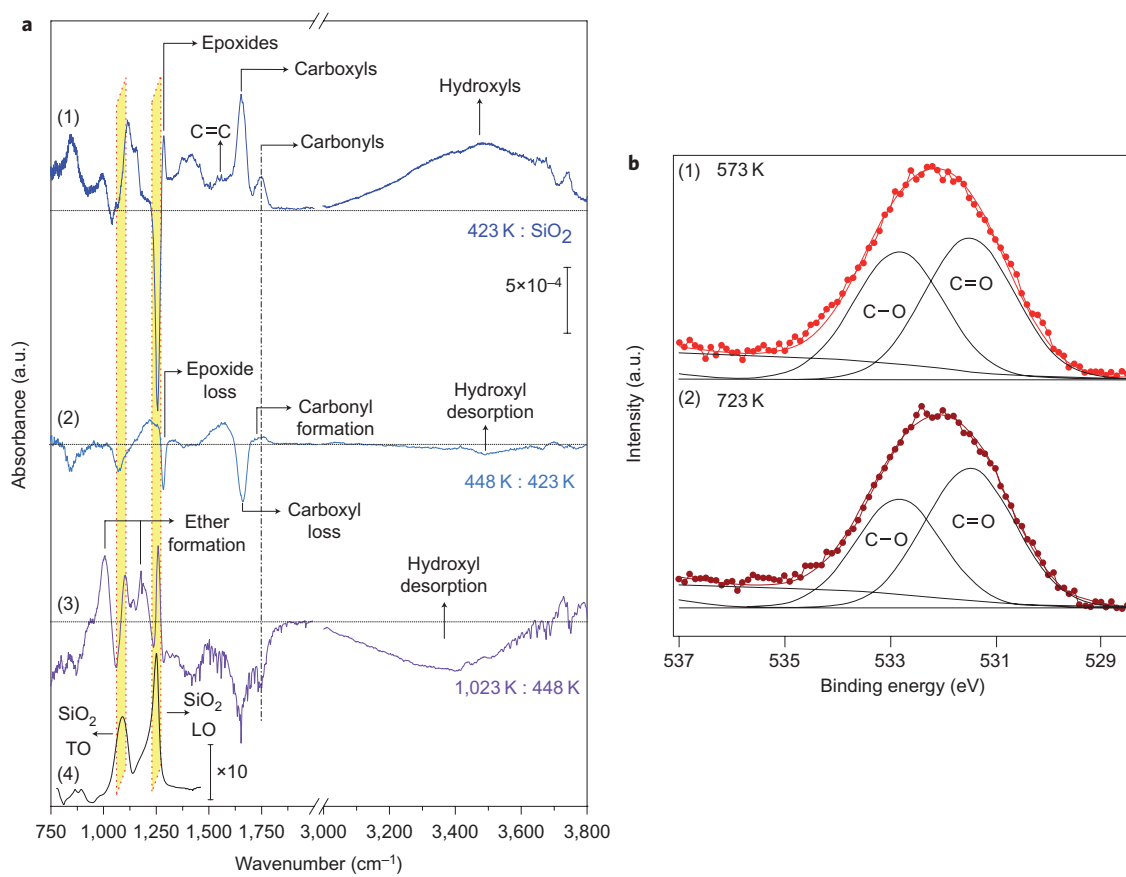


Figure 4 | In-situ transmission infrared and XPS spectra of rGO. **a**, Absorbance spectra of single-layer GO. After annealing at 423 K and referenced to the bare oxidized silicon substrate the spectrum (1) shows hydroxyls (broad peak at 3,050–3,800 cm⁻¹), carbonyls (1,750–1,850 cm⁻¹), carboxyls (1,650–1,750 cm⁻¹), C=C (1,500–1,600 cm⁻¹) and ethers and/or epoxides (1,000–1,280 cm⁻¹). The differential spectrum after annealing to 448 K (2), referenced to spectrum (1), indicates epoxide loss, carbonyl formation and hydroxyl desorption. The differential spectrum after annealing to 1,023 K (3), referenced to spectrum (2), shows ether formation (1,000–1,060 cm⁻¹ and 1,080–1,240 cm⁻¹) and hydroxyl desorption. The horizontal grey lines show the baseline in the differential spectra. The absorbance spectrum referenced to H-terminated silica (4) shows the full SiO₂ absorption of the oxide (range 750–1,500 cm⁻¹), characterized by longitudinal optical (LO, 1,250 cm⁻¹) and transverse optical (TO, 1,060 cm⁻¹) vibrational modes. **b**, O 1s XPS spectra collected on a single-layered GO thin film deposited on Au (10 nm)-SiO₂ (300 nm)-Si and annealed in an ultrahigh vacuum at the indicated temperatures for 15 minutes. By deconvolving the O 1s peaks collected after heating at 573 K (1) and 723 K (2), two components were identified as C=O bonds (533 eV) and C=O (531.2 eV) bonds^{20,43}. It was found that 50% of the oxygen atoms were in C=O configurations.

strain-free structure that results in a lower formation energy compared to that for the epoxy pair. Multiple interactions can also lead to stable, highly oxygenated hexagons, such as pyrones, 1,2-quinones and 1,4-quinones (Fig. 1g–i).

Carbon-vacancy generation involves a higher barrier energy in comparison to carbonyl formation and hence it occurs at higher temperatures. Evidence of this was the presence of larger amounts (18%) of residual furans and pyrans for low oxygen contents (16.6–20%) after annealing at 3,000 K (not shown), as compared to ~1–2% and <1% at 1,500 K and 1,000 K, respectively (Fig. 2). For a 33% initial oxygen concentration with a hydroxyl/epoxy ratio of 2/3 annealed at 1,600 K, a highly distorted honeycomb lattice caused by the evolution of ~2% of carbon atoms was observed. This led to the formation of cyclopentane rings and ether rings. In such cases, the overall concentration of the remaining oxygen was found to have 10% ether rings and 55% carbonyl groups.

Based on our MD simulations, we concluded that hydroxyls desorb at low annealing temperatures to leave the graphitized lattice intact. The epoxy groups require higher energy for desorption and thus are likely to remain if isolated, even for annealing at moderate temperatures. Interplay between epoxy groups and hydroxyls leads to incorporation of oxygen in-plane as ether groups or out-of-plane as carbonyl groups. Also, an increase in the annealing

temperature did not lead to an enhancement in the rate of oxygen release. On the contrary, at high annealing temperatures the probability of oxygen incorporation, as stable carbonyl groups and ether rings, was found to be higher. This is consistent with our recent experimental results⁶. Thus, from our calculations, it is clear that high-temperature annealing does not always lead to oxygen desorption.

Given these MD simulations results, we monitored the presence and evolution of oxygen species in GO using infrared absorption spectroscopy. The GO thin films utilized for infrared and XPS analysis in this work were identical to those analysed in detail by us previously⁶. After thermal treatment for five minutes, each infrared spectrum was measured at 333 K (Fig. 4a). The initial absorbance spectrum (1) was obtained after a mild anneal (423 K) to remove solvents and physisorbed species (for example, H₂O). The two areas highlighted in yellow (Fig. 4a, spectrum (4)) indicate a spectral region that is uncertain because of changes in the SiO₂ substrate onto which the GO was deposited. After this mild anneal (423 K), the pristine GO was composed of hydroxyls (broad peak at 3,050–3,800 cm⁻¹), carbonyls (1,750–1,850 cm⁻¹), carboxyls (1,650–1,750 cm⁻¹) (refs 15–16,29), C=C (1,500–1,600 cm⁻¹) and ethers and/or epoxides (1,000–1,280 cm⁻¹). After annealing to 448 K for five minutes, the differential spectrum (Fig. 4a, spectrum (2))

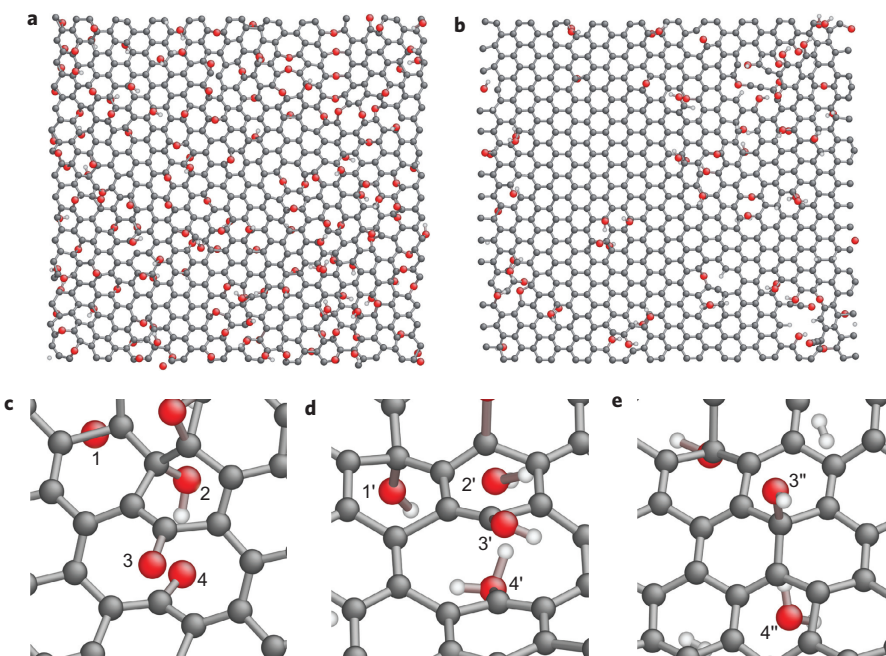


Figure 5 | Improvement in reduction efficiency on annealing of rGO in a hydrogen atmosphere. **a,b,** Structure of rGO after annealing at 1,500 K (**a**) (the initial GO had 25% oxygen and a hydroxyl/epoxy ratio of 3/2, and the structure is shown in Supplementary Fig. S2a) and after annealing the configuration from (**a**) in hydrogen (**b**). **c–e,** The evolution of residual oxygen groups during annealing of rGO in a hydrogen atmosphere leads to healing of the holes. The epoxy group labelled 1 in (**c**) evolves to a hydroxyl group (1') in (**d**). The hydroxyl group labelled (2) leaves the basal plane in the form of a water molecule (2'). The carbonyl labelled 3 in (**c**) is converted into a phenol (3') in (**d**) and then into a hydroxyl (3'') in (**e**). The carbonyl labelled (4) leaves the basal plane in the form of a water molecule (4'), which leads to the healing of the hole and the restoration of sp^2 bonding in the basal plane.

indicated that the carboxyl groups (from sample preparation and/or edge termination) were removed. Importantly, the intensities of the bands assigned to epoxides and hydroxyls weakened substantially. Correspondingly, close examination of the intensity of the carbonyl modes at $\sim 1,800\text{ cm}^{-1}$ indicated that it appeared to increase. The horizontal grey lines (Fig. 4a) show the baseline in the differential spectra, so the positive band that corresponds to the formation of carbonyl groups at 423 K is obvious. Indeed, the formation of carbonyls is seen clearly as a positive contribution within a large temperature range. The loss of epoxide and carboxyls could be observed in this temperature range as well. Experimental observations are therefore consistent with the mechanism proposed from the calculations. At higher temperatures (from 448 K up to 1,023 K (Fig. 4a, spectrum (3))), hydroxyls disappeared continuously and some ether groups were formed. Hydroxyls were not detected in infrared spectra at temperatures above 773 K.

The energy mode found from MD simulations for ether functional groups was compatible with substitutional oxygen in hexagonal and pentagonal rings, consistent with structures such as pyrans and furans, respectively. Although it was not possible to isolate the contributions from these species in the infrared spectra, the broad intensity increase between 1,000 and $1,280\text{ cm}^{-1}$ is consistent with the formation of pyrans and furans. After high-temperature annealing at 1,023 K, residual oxygen was observed in the form of ether groups ($1,000\text{--}1,060\text{ cm}^{-1}$ and $1,080\text{--}1,240\text{ cm}^{-1}$), as suggested from MD simulations. This ether group region was difficult to analyse because of the interference caused by changes in the longitudinal optical ($1,250\text{ cm}^{-1}$) and transverse optical ($1,060\text{ cm}^{-1}$) modes of the SiO_2 substrate, where the peaks of rGO ether groups are located.

The amount of oxygen-forming double bonds to carbon estimated by XPS is also compatible with the amount predicted by MD simulations. By deconvolving the O 1s peak (Fig. 4b), collected from the single-layered GO thin film after heating at 573 K

(Fig. 4b,i), and 723 K (Fig. 4b,ii), it was found that 50% of the oxygen was incorporated as $\text{C}=\text{O}$. This concentration is higher than that expected for carbonyls and carboxyls only present at the edges of GO sheets. Excluding contamination, as the annealing was carried out in an ultrahigh vacuum (10^{-10} mbar) and the Fourier transform infrared (FTIR) spectroscopy clearly showed complete desorption of H_2O below 423 K, carbonyl formation is likely to be consistent with the MD simulations observations (Fig. 2a) described above, which indicate an average carbonyl concentration of 45% after annealing at 1,500–1,600 K. Also, carbonyls and hydroxyls in the form of ketone and phenol groups were observed in NMR spectroscopy studies reported by Szabó *et al.*², which provides further confirmation of our theoretical predictions.

Based on our detailed calculations, several pathways for a more efficient reduction of GO to limit the formation of carbonyl and ether groups can be suggested. The calculations clearly point to the highly strained epoxy groups as the primary cause for the evolution of CO and CO_2 , which leads to holes and the formation of stable, planar residual oxygen in rGO. Therefore, if the concentration of epoxy groups in as-synthesized GO can be reduced in favour of that for hydroxyl groups, then the evolution of oxygen during reduction can occur with minimal perturbation to the grapheme basal plane. Specifically, we show here, using MD simulations, that a more efficient reduction along with healing of the rGO may be achieved through hydrogen treatment. The structure of rGO annealed in a hydrogen atmosphere is shown in Fig. 5b. From the data in Table 1, it can be seen that the oxygen concentration can be decreased even further by reheating the rGO up to 1,000 and 1,500 K in a hydrogen atmosphere (see Methods). There are three mechanisms for the increase in reduction using hydrogen, as indicated in Fig. 5. The first is the evolution of residual carbonyl pairs through the formation of water molecules and hydroxyl groups and rearrangement of the carbon atoms in the grapheme sp^2 configuration, which leads to the healing of holes formed

by the carbonyl pair (Fig. 5c–e). The second is the formation of hydroxyl groups with residual ether and epoxy groups in the presence of a hydrogen atmosphere (Fig. 5c,d) and the subsequent evolution of the hydroxyl functional groups by thermal annealing without introducing additional defects. Finally, residual hydroxyl groups are released from the basal plane by the formation of water molecules (Fig. 5c,d). Although annealing as-synthesized GO in a hydrogen atmosphere was shown to yield mixed results^{3,30,31}, to the best of our knowledge reheating rGO in hydrogen has not been reported in the literature. The insight gained from our theoretical work suggests that the optoelectronic properties of rGO can be improved significantly with careful design of the reduction treatment.

Finally, in addition to clarifying the nature of residual functional groups, we also observed the formation of stable linear chains of *sp*-bonded carbon atoms in the simulated rGO structure (see Fig. 1d). These carbon linear chains were obtained experimentally through a chemical route³² as well as by high-temperature and high-pressure treatment³³. Additionally, their formation and stability was predicted by density functional theory (DFT) simulations³⁴ of pristine nanoflakes of graphene heated at high temperatures. Very recently, stable and rigid carbon atomic chains were realized experimentally by removing carbon atoms row by row from graphene through controlled energetic electron irradiation inside a transmission electron microscope³⁵. The observation that carbon linear chains are formed during the deoxygenation of GO is interesting and could be a route to access their fundamental properties using the graphene sheet as a parent phase. In addition to the chains, other interesting features, such as triangular and pentagonal arrangements of carbon atoms, were observed (see Fig. 1j,k).

Conclusions

In summary, we report a MD simulations study of evolution of GO structure on thermal annealing. Our results provide insight into the fundamental problem that limits the device performance of rGO, the nature of persistent residual oxygen that remains in rGO despite aggressive chemical and thermal treatments. The MD simulations clearly reveal the formation of carbonyl and ether groups through transformation of the initial hydroxyl and epoxy groups during thermal annealing. The calculations show that hydroxyl groups desorb at low temperatures without altering the graphene basal plane. Isolated epoxy groups are relatively more stable, but substantially distort the graphene lattice on desorption. The simulations indicate that removal of carbon from the graphene plane is more likely to occur when the initial hydroxyl and epoxy groups are in close proximity to each other. The reaction pathway during thermal annealing between two nearby functional groups leads to the formation of carbonyl and ether groups, which are thermodynamically very stable. The theoretical results are corroborated by FTIR spectroscopy and XPS experiments. There is very good agreement between the calculations and experimental results. Our analysis suggests that careful reduction processes must be designed if highly ordered ('graphitized') graphene is to be obtained from GO.

Methods

Modelling. MD simulations were performed using the reactive force-field ReaxFF, which is a general bond-order dependent potential that provides accurate descriptions of bond breaking and bond formation in hydrocarbon–oxygen systems³⁶. To account for non-bonded interactions, such as van der Waals and Coulomb interactions for a system with changing connectivity, these interactions were calculated between every pair of atoms, irrespective of connectivity, and any excessive close-range, non-bonded interactions were avoided by the inclusion of a shielding term³⁶. For simulations on a number of hydrocarbon–oxygen systems^{37,38}, it was found that ReaxFF gave energies, transition states, reaction pathways and reactivity trends that are in agreement with quantum mechanical calculations and experiments.

To study the evolution of different functional groups on GO during high-temperature thermal reduction in an inert atmosphere (a vacuum), we first considered a 4.3 nm × 4 nm graphene sheet with randomly distributed epoxy and

hydroxyl functional groups on the two sides of the sheet. We implemented periodic boundary conditions along the graphene basal plane to avoid any edge effects. Once the initial groups were distributed as explained in the main text, the GO sheet was heated slowly from 10 K to a typical reduction temperature (in the range 1,000–3,000 K) over a time span of 250 fs. The temperature of the system was obtained by applying the thermostat to the entire system, that is to all the atoms. Therefore, according to the equipartition theorem, the kinetic energy of any given atom is $3/2 kT$. Thus, local effects where reactions take place do not influence the results. Then the system was annealed at this temperature for a time period that ranged from 25 ps to 250 ps to identify all the possible configurations of functional groups in rGO. In most of our simulations, we did not find any significant change in the morphology of the sheets after about 200 ps of annealing. Finally, to confirm the stability of the configurations obtained as a result of high-temperature thermal reduction, rGO sheets were annealed at 300 K for 1.25 ps. These simulations were performed in a canonical moles (N), volume and temperature (NVT) ensemble with a Berendsen thermostat for temperature control and a time step of 0.25 fs. The simulated hydrogen treatment was performed on both sides of the GO sheet. The concentration of the hydrogen was 15% of the carbon atoms in GO. The temperature was increased up to 1,000 or 1,500 K in 250 fs and held at that temperature for 50 ps. The hydrogen that did not participate in any chemical reactions, any by-products were removed and the system was quenched to room temperature in 1.25 ps. Finally, the system was annealed at room temperature for an additional 1.25 ps.

The first-principles DFT calculations to compute the formation energies of epoxy, carbonyl and phenol configurations shown in Fig. 3 were performed with a plane-wave basis set using the *ab initio* simulation package VASP^{39,40}. We used projector-augmented wave potentials⁴¹ to represent the ionic cores. A generalized gradient approximation of the Perdew–Burke–Ernzerhof⁴² form was used for the exchange and correlation functional. We implemented a kinetic energy cutoff at 500 eV. To compute the total energy of the structures in Fig. 3 we used a periodic simulation cell with 120 carbon atoms and a 12 Å thick vacuum region in the direction normal to the graphene sheet. These structures were then relaxed using the conjugate gradient algorithm until the atomic forces were smaller than 0.01 eV Å^{−1}.

GO thin films. For the infrared absorption studies, GO samples were deposited on oxidized silicon substrates (oxide ~1.5 nm thick, wafer polished on both sides), with dimensions 3.8 × 1.5 cm (1.5 × 0.6 in). The GO thin films used for FTIR spectroscopy and XPS were deposited by the vacuum filtration method⁵ from a GO solution prepared using the modified Hummers procedure (details of which are included in the Supplementary Information of Eda *et al.*⁵). The GO-coated silica sample was held by two tantalum clips (for direct resistive heating) and placed in a vacuum chamber ($\sim 10^{-5}$ torr base pressure). The measurements were taken using a ThermoFisher Nicolet 6700 FT-IR spectrometer (KBr beam splitter) with a deuterated triglycine sulfate detector under a constant nitrogen purge of 20 cm³ min^{−1}. The optimum conditions were chosen as an optical velocity of 0.6329 cm s^{−1} with an incidence angle of 70° using direct transmission. The samples were heated through the current control by using 6010 A d.c. power supply (0–200 V/0–17 A, 1,000 W, Hewlett Packard) with a temperature control using Eurotherm. The reference for most spectra, unless specifically listed as differential spectra, was the original oxidized silicon sample. Hence, any perturbation of the original oxide during GO deposition, including sample cleaning prior to deposition, is reflected in the spectra, mostly as a loss of SiO₂.

Received 12 January 2010; accepted 21 April 2010;
published online 6 June 2010

References

1. Stankovich, S. *et al.* Graphene-based composite materials. *Nature* **442**, 282–286 (2006).
2. Szabó, T. *et al.* Evolution of surface functional groups in a series of progressively oxidized graphite oxides. *Chem. Mater.* **18**, 2740–2749 (2006).
3. Wang, X., Zhi, L. & Mullen, K. Transparent, conductive graphene electrodes for dye-sensitized solar cells. *Nano Lett.* **8**, 323–327 (2007).
4. Becerril, H. A. *et al.* Evaluation of solution-processed reduced graphene oxide films as transparent conductors. *ACS Nano* **2**, 463–470 (2008).
5. Eda, G., Fanchini, G. & Chhowalla, M. Large-area ultrathin films of reduced graphene oxide as a transparent and flexible electronic material. *Nature Nanotech.* **3**, 270–274 (2008).
6. Mattevi, C. *et al.* Evolution of electrical, chemical, and structural properties of transparent and conducting chemically derived graphene thin films. *Adv. Funct. Mater.* **19**, 2577–2583 (2009).
7. Jung, I., Dikin, D. A., Piner, R. D. & Ruoff, R. S. Tunable electrical conductivity of individual graphene oxide sheets reduced at 'low' temperatures. *Nano Lett.* **8**, 4283–4287 (2008).
8. Gómez-Navarro, C. *et al.* Electronic transport properties of individual chemically reduced graphene oxide sheets. *Nano Lett.* **7**, 3499–3503 (2007).
9. Neto, A. H. C., Guinea, F., Peres, N. M. R., Novoselov, K. S. & Geim, A. K. The electronic properties of graphene. *Rev. Mod. Phys.* **81**, 109–162 (2009).
10. Du, X., Skachko, I., Barker, A. & Andrei, E. Y. Approaching ballistic transport in suspended graphene. *Nature Nanotech.* **3**, 491–495 (2008).

11. Stankovich, S. *et al.* Synthesis of graphene-based nanosheets via chemical reduction of exfoliated graphite oxide. *Carbon* **45**, 1558–1565 (2007).
12. Bourlinos, A. B. *et al.* Graphite oxide: chemical reduction to graphite and surface modification with primary aliphatic amines and amino acids. *Langmuir* **19**, 6050–6055 (2003).
13. Hyeon-Jin, S. *et al.* Efficient reduction of graphite oxide by sodium borohydride and its effect on electrical conductance. *Adv. Funct. Mater.* **19**, 1987–1992 (2009).
14. Lerf, A., He, H., Forster, M. & Klinowski, J. Structure of graphite oxide revisited. *J. Phys. Chem. B* **102**, 4477–4482 (1998).
15. Szabó, T., Berkesi, O. & Dékány, I. DRIFT study of deuterium-exchanged graphite oxide. *Carbon* **43**, 3186–3189 (2005).
16. Fuente, E., Menendez, J. A., Diez, M. A., Suarez, D. & Montes-Moran, M. A. Infrared spectroscopy of carbon materials: a quantum chemical study of model compounds. *J. Phys. Chem. B* **107**, 6350–6359 (2003).
17. Nakajima, T. & Matsuo, Y. Formation process and structure of graphite oxide. *Carbon* **32**, 469–475 (1994).
18. Ulrich, H. & Rudolf, H. Über die säurenatur und die methylierung von graphitoxid. *Ber. Dtsch Chem. Ges.* **72**, 754–771 (1939).
19. Scholz, W. & Boehm, H. P. Untersuchungen am graphitoxid. VI. Betrachtungen zur struktur des graphitoxids. *Z. Anorg. Allg. Chem.* **369**, 327–340 (1969).
20. Honoria-Lucas, C., López-Peinado, A. J., de López-González, J. D., Rojas-Cervantes, M. L. & Martín-Aranda, R. M. Study of oxygen-containing groups in a series of graphite oxides: physical and chemical characterization. *Carbon* **33**, 1585–1592 (1995).
21. Brodie, B. C. On the atomic weight of graphite. *Phil. Trans. R. Soc. Lond.* **149**, 249–259 (1859).
22. Staudenmaier, L. Verfahren zur darstellung der graphitsaure. *Ber. Dtsch Chem. Ges.* **31**, 1481–1487 (1898).
23. Hummers, W. S. & Offeman, R. E. Preparation of graphitic oxide. *J. Am. Chem. Soc.* **80**, 1339 (1958).
24. Dreyer, D. R., Park, S., Bielawski, C. W. & Ruoff, R. S. The chemistry of graphene oxide. *Chem. Soc. Rev.* **38**, 228–240 (2010).
25. Cassagneau, T., Guerin, F. & Fendler, J. H. Preparation and characterization of ultrathin films layer-by-layer self-assembled from graphite oxide nanoplatelets and polymers. *Langmuir* **16**, 7318–7324 (2000).
26. Szabó, T., Tombácz, E., Illés, E. & Dékány, I. Enhanced acidity and pH-dependent surface charge characterization of successively oxidized graphite oxides. *Carbon* **44**, 537–545 (2006).
27. Cai, W. *et al.* Synthesis and solid-state NMR structural characterization of ¹³C-labeled graphite oxide. *Science* **321**, 1815–1817 (2008).
28. He, H., Klinowski, J., Forster, M. & Lerf, A. A new structural model for graphite oxide. *Chem. Phys. Lett.* **287**, 53–56 (1998).
29. Hadzi, D. & Novak, A. Infra-red spectra of graphitic oxide. *Trans. Faraday Soc.* **51**, 1614–1620 (1955).
30. Wang, S. *et al.* High mobility, printable, and solution-processed graphene electronics. *Nano Lett.* **10**, 92–98 (2010).
31. López, V. *et al.* Chemical vapor deposition repair of graphene oxide: a route to highly-conductive graphene monolayers. *Adv. Mater.* **21**, 4683–4686 (2009).
32. Rubin, Y., Knobler, C. B. & Diederich, F. Precursors to the cyclo[n]carbons: from 3,4-dialkynyl-3-cyclobutene-1,2-diones and 3,4-dialkynyl-3-cyclobutene-1,2-diols to cyclobutenodehydroannulenes and higher oxides of carbon. *J. Am. Chem. Soc.* **112**, 1607–1617 (2002).
33. Ravagnan, L. *et al.* Cluster-beam deposition and *in situ* characterization of carbyne-rich carbon films. *Phys. Rev. Lett.* **89**, 285506 (2002).
34. Amanda, S. B. & Ian, K. S. Thermal stability of graphene edge structure and graphene nanoflakes. *J. Chem. Phys.* **128**, 094707 (2008).
35. Jin, C., Lan, H., Peng, L., Stuenaga, K. & Iijima, S. Deriving carbon atomic chains from graphene. *Phys. Rev. Lett.* **102**, 205501 (2009).
36. van Duin, A. C. T., Dasgupta, S., Lorant, F. & Goddard, W. A. ReaxFF: a reactive force field for hydrocarbons. *J. Phys. Chem. A* **105**, 9396–9409 (2001).
37. Chenoweth, K., Cheung, S., van Duin, A. C. T., Goddard, W. A. & Kober, E. M. Simulations on the thermal decomposition of a poly(dimethylsiloxane) polymer using the ReaxFF reactive force field. *J. Am. Chem. Soc.* **127**, 7192–7202 (2005).
38. Chenoweth, K., van Duin, A. C. T. & Goddard, W. A. ReaxFF reactive force field for molecular dynamics simulations of hydrocarbon oxidation. *J. Phys. Chem. A* **112**, 1040–1053 (2008).
39. Kresse, G. & Furthmüller, J. Efficient iterative schemes for *ab initio* total-energy calculations using a plane-wave basis set. *Phys. Rev. B* **54**, 11169–11186 (1996).
40. Kresse, G. & Furthmüller, J. Efficiency of *ab initio* total energy calculations for metals and semiconductors using a plane-wave basis set. *Comput. Mater. Sci.* **6**, 15–50 (1996).
41. Kresse, G. & Joubert, D. From ultrasoft pseudopotentials to the projector augmented-wave method. *Phys. Rev. B* **59**, 1758–1775 (1999).
42. Perdew, J. P., Burke, K. & Ernzerhof, M. Generalized gradient approximation made simple. *Phys. Rev. Lett.* **77**, 3865–3868 (1996).
43. Zhang, J. *et al.* Surface-modified carbon nanotubes catalyze oxidative dehydrogenation of *n*-butane. *Science* **322**, 73–77 (2008).

Acknowledgements

We acknowledge support from the National Science Foundation (NSF) and Nanoelectronic Research Initiative through the Brown University Materials Research Science and Engineering Center program and from the NSF through grants CMMI-0825771 and CMMI-0855853. We thank N. Medhekar, R. Grantab and I. Milas for discussions and suggestions. Computational support for this research was provided by the grant TG-DMR090098 from the TeraGrid advanced support program and the Center for Computation and Visualization at Brown University. M.C. and C.M. acknowledge financial support from the Jacobs Chair Funds at Rutgers University and an NSF CAREER Award (ECS 0543867). The work at University of Texas Dallas was supported by the SWAN-NRI program and Texas Instruments.

Author contributions

V.B.S. and M.C. conceived the project, A.B. and V.B.S. conducted the MD simulations and first-principles calculations with input from C.M. and M.C., M.A. and Y.C. performed the FTIR spectroscopy measurements and analysis, M.C., C.M. and V.B.S. wrote the manuscript with input from Y.C. and M.A. All of the authors read and approved the contents of the manuscript prior to submission. A.B. and C.M. contributed equally to this work.

Additional information

The authors declare no competing financial interests. Supplementary information accompanies this paper at www.nature.com/naturechemistry. Reprints and permission information is available online at <http://npg.nature.com/reprintsandpermissions/>. Correspondence and requests for materials should be addressed to V.B.S.